Wave Haptics: Encoderless Virtual Stiffnesses

Günter Niemeyer[1], Nicola Diolaiti[2], Neal Tanner[1]

[1]*Telerobotics Lab, Stanford University*
gunter.niemeyer@stanford.edu
tanner@stanford.edu

[2]*DEIS, University of Bologna AI-Robotics Lab, Stanford University*
ndiolaiti@deis.unibo.it

Abstract

Haptic rendering commonly implements virtual springs using DC motors with current amplifiers and encoder-based position feedback. In these schemes, quantization, discretization, and delays all impose performance limits. Meanwhile the amplifiers try to cancel the electrical motor dynamics, which are actually beneficial to the haptic display.

We present an alternate approach that fully embraces and utilizes all electrical dynamics, following two insights: First, the electrical inductance L can serve as a stiffness, providing a natural sensor-less coupling between the virtual environment and the user. Second, the electrical resistance R can serve as part of a wave transformation. Implementing virtual objects in a wave domain provides complete robustness to servo delays or discretization.

The resulting system requires only a simple voltage drive circuit. Built upon the physical behaviors, if can outperform traditional approaches achieving higher virtual stiffness. Encoder feedback is only required for absolute position information, with damping and velocity information inherently available from back-EMF effects. A prototype system has been implemented and confirms the promise of this novel paradigm.

I. Introduction

Stable implementation of stiff virtual environments remains a challenge for kinesthetic force feedback devices with impedance causality. In particular, the traditional approach consists of a digital control loop using discretized and quantized position readings, as seen in Fig. 1. Force is actuated by means of a DC motor controlled by a current amplifier, in turn fed by a constant force command during each servo cycle.

It has been recognized that the maximum achievable stiffness with such an approach is limited by the lack of information to the controller caused

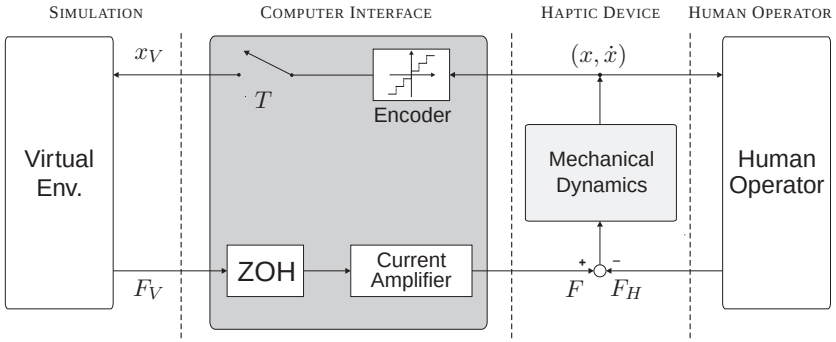

Fig. 1. The traditional implementation of stiff virtual environments

by time discretization [1], [2] and position quantization [3], [4] related to the use of encoders as position sensors. Therefore the intrinsic friction of the device and possibly the damping added by user's grasp become essential in stabilizing the haptic rendering. In effect, the virtual environment can only be rendered for a limited frequency range. Alternatively, the use of analog position measurements and time continuous feedback has been explored in [5]. The electrical current amplifiers include their own internal feedback to regulate the motor current. They aim to reject back-EMF while speeding up the L-R dynamics.

In the following we adopt a different perspective. We use the electrical resistance and back-EMF to implicitly obtain velocity information and enable appropriate viscous damping. We also use the electrical inductance to create a stiffness. Built out of natural dynamics, these effects are always available at high frequency together with the controlled lower frequencies, creating performance beyond traditional approaches. Furthermore, using a wave variable description borrowed from telerobotics, the implementation is entirely insensitive to servo delays.

II. Exploiting the Motor Dynamics

Though generally ignored under the assumptions of an ideal actuator and perfect current amplification, the electrical motor dynamics are well known to be:

$$\begin{aligned} e_A(t) &= Ri(t) + L\frac{di(t)}{dt} + e_{BE}(t) \\ e_{BE}(t) &= k_T\dot{x}(t) \end{aligned} \tag{1}$$

where e_A is the applied voltage to the armature circuit consisting of the resistance R, the inductance L and the back-EMF voltage e_{BE}. The

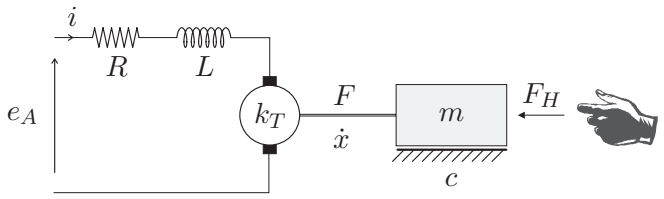

Fig. 2. The electrical and mechanical DC motor dynamics

mechanical dynamics are given as:

$$\begin{aligned} m\ddot{x}(t) &= F(t) - c(\dot{x}(t)) - F_H(t) \\ F(t) &= k_T i(t) \end{aligned} \tag{2}$$

where m is the rotor inertia, c is the (nonlinear) friction and F_H is the user torque *opposing* the motion $\dot{x}$ of the rotor. The torque constant and back-EMF constant are the same physical parameter and are both denoted by k_T. The equations are illustrated in Fig. 2 and represented in block diagram form in Fig. 3.

The actuator converts electrical into mechanical energy and thus the elements R and L can be easily mapped into the mechanical domain. For example, it is well known that the back-EMF voltage together with the resistance can be used to increase the apparent viscous friction [6] or to obtain an accurate measurement of the velocity. The resistance R maps

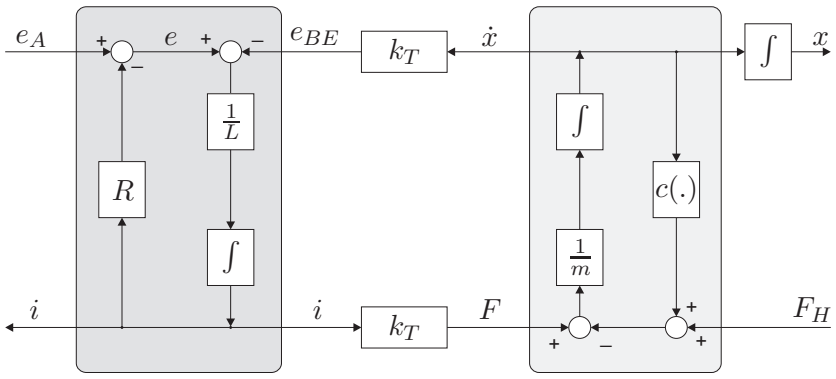

Fig. 3. Block diagram of the DC motor dynamics

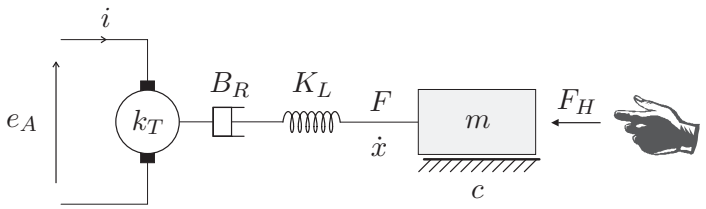

Fig. 4. Rotor inductance L and resistance R can be interpreted as series connection of a spring $K_L = {k_T}^2/L$ and a viscous damper $B_R = {k_T}^2/R$

into a mechanical viscous damper

$$B_R = \frac{{k_T}^2}{R} \tag{3}$$

Similarly, the inductance L provides energy storage and can be interpreted as a spring of stiffness:

$$K_L = \frac{{k_T}^2}{L} \tag{4}$$

The equivalent spring and damper are connected in series between the rotor inertia and the energy conversion element, as seen in Fig. 4. Because of the series connection, the damper dominates the low frequency behavior and the stiffness is often overlooked.

With low inductance motors commonly used in haptics, K_L creates a very high stiffness. For example, for the Maxon RE 25 motors found in the PHANToM 1.0 with values of $k_T = 43.8$ mNm/A and $L = 0.83$ mH, we have $K_L = 2.31$ Nm/rad. With an approximate $8:1$ gear ratio and lever arm of 14 cm the corresponding tip stiffness reaches 7500 N/m. For comparison, the maximum stable value of a virtual spring implemented according to the scheme of Fig. 1 has been found to be approximately 1100 N/m [4].

Therefore, it is worthy to develop a control scheme that takes advantage of the *built-in spring* present in each motor for the haptic rendering of stiff virtual environments. Since K_L is a *physical* element of the system, it is not affected by the non-idealities of the digital control loop that cause energetic inconsistencies and lead the system to instability. Moreover the force feedback it provides does not require any position sensing at all and operates at high frequencies.

III. Wave Variables for Haptic Rendering

For the purpose of designing a controller we consider the inductor as a series spring, retaining the resistance in the electrical domain as seen

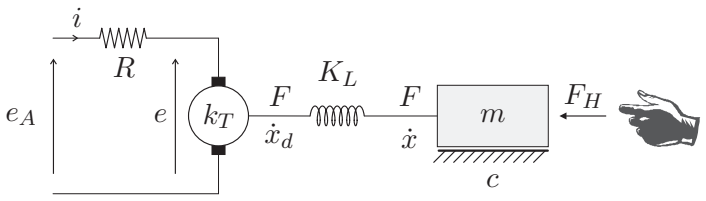

Fig. 5. Motor dynamics interpretation used in the controller design

in Fig. 5. The controller imposes motion

$$\dot{x}_d(t) = \frac{1}{k_T} e \tag{5}$$

on the spring corresponding to a voltage e. The controller represents a voltage drive and the current i indicates a measurement of the torque F.

We interpret the dissipative element as part of a natural wave transform [7], [8], as shown in Fig. 6. A wave transform encodes the normal power variables of velocity $\dot{x}$ and force F into wave variables u and v, without loss of information or change in power flow. The wave quantities inherently describe both signal and power flow and are thus unaffected by delays or lags. In this context, the wave variables as defined in [8] are given as:

$$\begin{aligned} v(t) &:= \frac{e - Ri}{\sqrt{2R}} = \frac{B_R \dot{x}_d - F}{\sqrt{2B_R}} \\ u(t) &:= \frac{e + Ri}{\sqrt{2R}} = \frac{B_R \dot{x}_d + F}{\sqrt{2B_R}} \end{aligned} \tag{6}$$

where $\dot{x}_d(t)$ is the desired spring motion and F denotes the spring force. The equivalent viscous damping B_R serves as the wave impedance. The

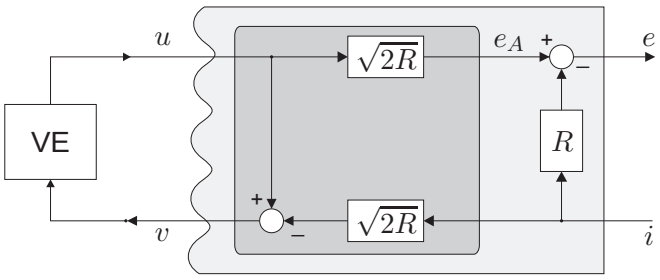

Fig. 6. Wave Transform connecting Virtual Environment VE to electrical domain

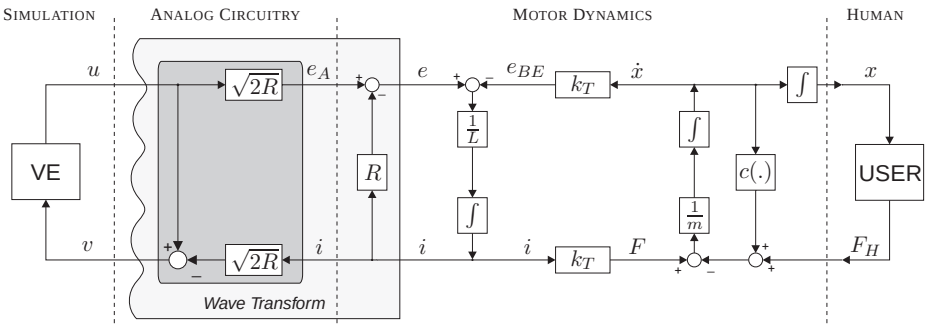

Fig. 7. Block diagram of a DC motor with the wave controller

overall instantaneous power $P(t)$ flowing from the virtual environment to the motor is:

$$P(t) = e(t)i(t) = \dot{x}_d(t)F(t) = \frac{1}{2}u^2(t) - \frac{1}{2}v^2(t) \tag{7}$$

so that a wave variable has units of square root of Watt.

To complete the wave transform, the dark shaded area of Fig. 6 showing the two $\sqrt{2R}$ gains and the summing junction is realized by means of an *analog circuitry*. This implements:

$$\begin{aligned} e_a &= \sqrt{2R}\,u \\ v &= u - \sqrt{2R}\,i \end{aligned} \tag{8}$$

The complete system is depicted in Fig. 7. The wave variables $u(t)$ and $v(t)$ encode the power exchanged with the motor by the simulated virtual environment. Since each wave variable carries its own power, the passivity of the interconnection is guaranteed as long as the modulus of the transfer function

$$D(s) = \frac{U(s)}{V(s)} \tag{9}$$

representing the virtual environment in wave space is at most the unity.

Because the wave variable $u(t)$ and $v(t)$ exist as real signals in the circuit, the virtual environment can be implemented in several ways. Simple transfer functions $D(s)$ can be realized in analog hardware. Alternatively, $v(t)$ and $u(t)$ can be digitized and the virtual environment implemented on a computer either in wave space or in traditional power variables by use of a second de-coding digital wave transformation. In either case, any time delays or phase lags due to the discretization are guaranteed not to affect the stability of the overall system.

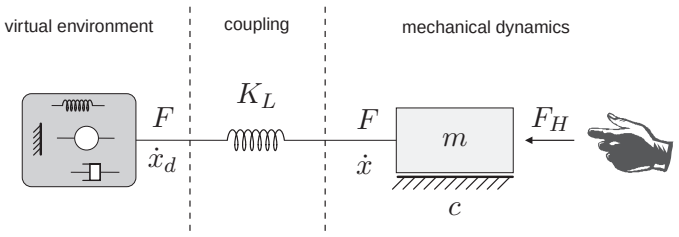

Fig. 8. The inductance acts as *physical* coupling with the virtual environment

IV. Interpretation

As discussed in detail in [7], wave variables can by used to describe an interconnection of elements. This gives us the ability to implement any passive virtual environment, with which the user interacts through the natural dynamics of the mechanical device and equivalent spring K_L. The latter can therefore be interpreted as a coupling element, resembling the virtual coupling concept of [9]. This coupling has the advantage of being a physical element and is not affected by the stability issues of a digital implementation. This interpretation leads to the conceptual scheme of Fig. 8.

The two most extreme passive environments are free motion and rigid contact. Both imply an infinite frequency response, as motion occurs immediately for any force in the former and forces are immediately created for any motion in the latter. Causality of an impedance device clearly favors free motion and challenges rendition of rigid contact.

In the wave domain, both of these environments are easily expressed. Free motion avoids all forces ($F = 0$) and reflects all power carried by the incoming wave $v(t)$ back by means of $u(t)$ as:

$$u(t) = v(t) \qquad \Longleftrightarrow \qquad i = 0 \quad \forall\, e \quad \text{or} \quad F = 0 \quad \forall\, \dot{x}_d \tag{10}$$

where (6) converts the wave relation into the power variable description.

Dually, a rigid contact also reflects all power by suppressing any motion ($\dot{x}_d = 0$) as:

$$u(t) = -v(t) \qquad \Longleftrightarrow \qquad e = 0 \quad \forall\, i \quad \text{or} \quad \dot{x}_d = 0 \quad \forall\, F \tag{11}$$

Note this does not hold the applied voltage e_A at zero, but only cancels the voltage across the inductor and back-EMF. It does not short the motor, instead effectively sets $e_A = Ri$. Illustrated in Fig. 9, it implies that K_L is the maximum stiffness that can be rendered to the user.

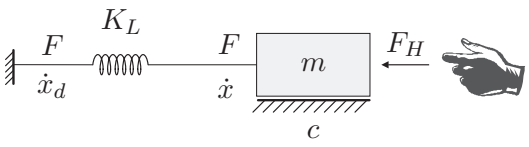

Fig. 9. Haptic interaction with a rigid virtual wall

A haptic simulation where the user experiences interactions with stiff bodies or unconstrained motion can be implemented as:

$$u(t) = \eta v(t) \qquad \text{where} \qquad \eta = \begin{cases} -1 & \text{in contact} \\ +1 & \text{in free motion} \end{cases} \tag{12}$$

To switch between these two values, a collision detection algorithm should take advantage of direct position measurements. An encoder is thus required to detect the collision with a unilateral constraint, but is not used to compute the force fed back to the user.

V. Implementation

Incorporating and utilizing the electrical dynamics, K_L is the maximum stiffness that can be rendered by means of a passive wave-haptic approach. Disturbances may stem from the unmodeled high frequency dynamics of the power transistors used to achieve the desired voltage input e_A, as well as from other sources of electrical noise in the control loop. These phenomena occur at much higher frequency (several hundred kilohertz) than the perceptual bandwidth of the human operator (about one kilohertz). To address these limitations, a high frequency low-pass wave filter

$$H(s) = \frac{\lambda}{s + \lambda} \tag{13}$$

can then be included in series with the virtual environment without significantly affecting the perceived transients [10]. Indeed such a filter retains passivity and adds a further series stiffness of

$$K_{filter} = \frac{{k_T}^2}{R}\ \lambda \tag{14}$$

which is significantly stiffer than the existing coupling of K_L. The transfer function $D(s)$ of the overall controller dynamics in the wave domain becomes:

$$D(s) = \eta\ \frac{\lambda}{s + \lambda}\ W(s) \tag{15}$$

where the magnitude of η can be further tuned in the interval $-1 \leq \eta \leq 1$ to remove power and introduce damping. Finally $W(s)$ may incorporate other dynamics into the simulated virtual environment.

We have implemented a simple prototype system using (12) and (15) with $\lambda = 10,000$ rad/sec, $\eta = \pm 1$, $W(s) = 1$. In particular, we use a Maxon RE25-118743 motor that features $K_L = 2.2815$ Nm/rad with the control electronics realized by means of analog circuitry. Power amplification is performed by a couple of complementary MOSFET transistors in a push-pull configuration and an analog switch alternates between free space (η=1) and rigid contact (η=-1). Power supply limits the current provided to the motor to 1 A. Data is collected at 5 kHz using A/D conversion and a high resolution encoder (10^4 counts per revolution) to measure the motor shaft position.

Consider contact against a stiff virtual wall located at $x_W = 0$. From the encoder reading, we derive a simple binary signal indicating penetration into the wall. This logic signal commands the analog switch and selects the appropriate behavior. Preliminary results are shown in Fig. 10 and 11. In Fig. 10 we see the circuit correctly renders the behavior of free space, since when $x < 0$ the feedback torque F is zero. The voltage e_A adjusts slightly to counter the back-EMF voltage. As contact is experienced, current and torque quickly rise to their maximum value before saturation intervenes at about $F \simeq 0.021$ Nm. Better viewed in Fig. 11, the stiffness rendered during the compression phase is approximately $K \simeq 1.9$ Nm/rad, in good agreement with the expectations from the previous analysis.

We note that the compression and the restitution phases appear asymmetric. This behavior is a direct consequence of voltage saturation, which is not yet included in the simple dynamics (1). When the drive voltage hits a fixed saturation limit, the back-EMF effects can not be properly canceled and the current is affected by motion. As the compression slows, the resisting force drops to its steady state value and, as motion begins during restitution, the restoring force drops accordingly. Effectively the spring forces are overlayed with the back-EMF's viscous damping.

As a second effect, the voltage modification caused by the saturation also shifts the endpoint x_d of the spring K_L. Recall from (5) that voltage implies motion, such that the desired behavior depicted in Fig. 9 reverts back to Fig. 4. Fortunately, as contact is broken, the behavioral switch via η resets the system for the next collision.

Finally, we find two issues that may require study for future implementations: First, knowledge of the motor resistance R is necessary to implement (8) and create the wave transformation (6) in a passive fashion.

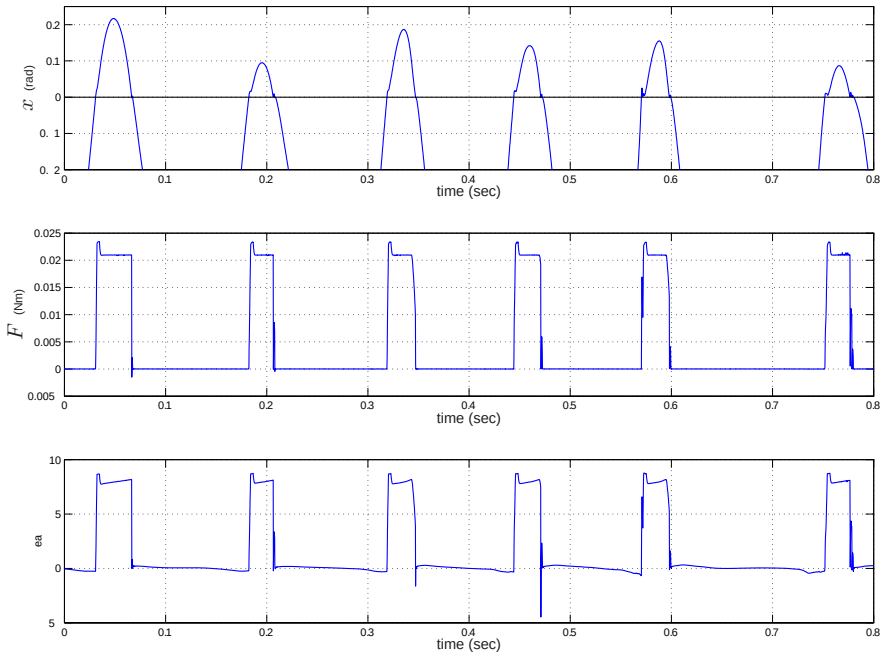

Fig. 10. Repeated contacts with the virtual wall: position, force and voltage diagrams

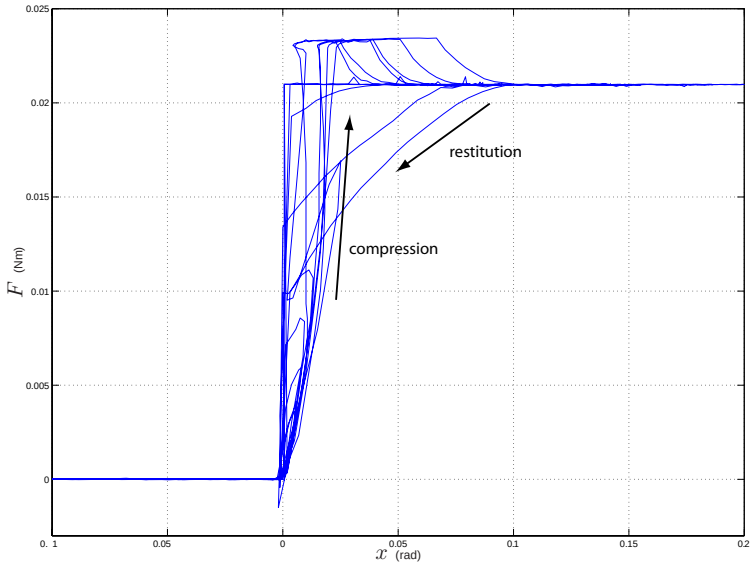

Fig. 11. Behavior of the feedback torque F during contact with the virtual wall

Inaccuracies lead to errors in the command voltage e_A and, as above, to drift. In particular, the resistance varies with temperature and adjustable circuitry may be required to compensate for this effect. Fortunately thermal dynamics are much slower than the dynamics involved in haptic rendering, so their influence on the stability of the overall scheme is marginal and drift may be negated by encoder feedback at a higher level. Finally, commutation in brushed DC motors introduces discontinuities into the simple dynamics (1) and may be perceived by the user. Application to brushless motors promises smoother operation.

VI. Conclusions

In this paper we propose to exploit the electrical dynamics of the DC motor used to render the force feedback in virtual reality applications. For the motors commonly used in this context, the equivalent stiffness of the motor inductance is higher than the stiffness that can be achieved by means of a classical digital control loop.

We propose to take advantage of this physical spring to render stiff virtual objects, avoiding the problems related to position quantization and time discretization. In this way, the usually neglected electrical dynamics are effectively used to improve performance. Realization by means of a reliable analog circuitry is possible entirely within the electrical domain. The required components include only a sense resistor to acquire i, two gain stages, and a summation stage depicted in Fig. 6. The voltage command e_A is applied directly to the motor via a power stage, replacing the more complex current amplifiers typically used.

The virtual environment is interfaced to the motor by means of wave variables and in this domain the time delays and phase lags caused by a discrete-time implementation do not affect the energy balance and therefore the stability of the overall system.

This approach is very appealing with its intrinsic simplicity and the better use it makes of the physical components of the haptic device. It does not require assumptions on the mechanical friction to obtain stability and passivity. Conversely, the passivity is obtained constructively and the effects of non-idealities are confined behind the wave variables transform, guaranteeing intrinsic robustness to servo delay.

Acknowledgments

N. Diolaiti gratefully acknowledges support for this research which was provided, in part, by NIH Grant R33 LM 007295 and by the AGI Corporation.

REFERENCES

[1] J. Colgate and G. Schenkel, "Passivity of a class of sampled-data systems: Application to haptic interfaces," in *American Control Conference*, Baltimore, Maryland, June 1994, pp. 3236–3240.

[2] B. Gillespie and M. Cutkosky, "Stable user-specific rendering of the virtual wall," in *ASME IMECE*, vol. DSC-Vol. 58, Atlanta, GA, November 1996, pp. 397–406.

[3] J. J. Abbott and A. M. Okamura, "A sufficient condition for passive virtual walls with quantization effects," in *ASME IMECE International Symposium on Advances in Robot Dynamics and Control*, 2004, in press.

[4] N. Diolaiti, G. Niemeyer, F. Barbagli, J. K. Salisbury, and C. Melchiorri, "The effect of quantization and coulomb friction on the stability of haptic rendering," in *WHC '05: Proceedings of the First Joint Eurohaptics Conference and Symposium on Haptic Interfaces for Virtual Environment and Teleoperator Systems (WHC'05)*. Pisa, Italy: IEEE Computer Society, March 2005, pp. 237–246.

[5] M. Kawai and T. Yoshikawa, "Haptic display with an interface device capable of continuous-time impedance display within a sampling period," *IEEE/ASME Transactions on Mechatronics*, vol. 9, no. 1, pp. 58–64, March 2004.

[6] J. S. Mehling, J. E. Colgate, and M. A. Peshkin, "Increasing the impedance range of a haptic display by adding electrical damping," in *WHC '05: Proceedings of the First Joint Eurohaptics Conference and Symposium on Haptic Interfaces for Virtual Environment and Teleoperator Systems (WHC'05)*. Washington, DC, USA: IEEE Computer Society, 2005, pp. 257–262.

[7] G. Niemeyer and J. Slotine, "Using wave variables for system analysis and robot control," in *Proceedings of the IEEE International Conference on Robotics and Automation*, vol. 2, Albuquerque, New Mexico, April 1997, pp. 1619–1625.

[8] G. Niemeyer and J. Slotine, "Telemanipulation with time delays," *International Journal of Robotics Research*, vol. 23, no. 9, pp. 873–890, September 2004.

[9] B. Miller, J. Colgate, and R. Freeman, "Environment delay in haptic systems," in *Proceedings of the IEEE International Conference on Robotics and Automation*, San Francisco, CA, April 2000, pp. 2434–2439.

[10] N. Tanner and G. Niemeyer, "Practical limitations of wave variable controllers in teleoperation," in *IEEE Conference on Robotics, Automation, and Mechatronis*, Singapore, 1-3 December 2004.